On the attempts to reduce parasitic viscous forces in the oil-air capillary bridge simulations

Kushal Manjunath[1], *Catherine* O'Sullivan[1], and *Mai* Sawada[1,2]

[1]Department of Civil and Environmental Engineering, Imperial College London
[2]Department of Civil and Environmental Engineering, Institute of Science, Tokyo

Abstract. Setting up a stable multiphase Volume of Fluid (VoF) numerical simulation to quantify capillary bridge forces acting on soil particles in the pendular regime presents significant computational challenges. Non-physical currents in these surface tension dominated simulations generate parasitic viscous forces that compromise the total force predictive capability of the numerical model. This study examines a two-sphere system with an intervening capillary bridge as its primary test case. OpenFOAM's Geometric (PLIC, isoAdvector) and Algebraic (MULES) VoF approaches using the CSF Surface Tension (ST) model proved insufficient, necessitating modifications to the ST model. Two specific advanced ST models for the algebraic VoF were investigated: Laplacian Smoothing (SCSF) and Sharpening with Smoothing (SSF) of the VoF field. The parameters of the ST model require tuning based on the specific fluid combination considered. For oil-air fluid combinations characterized by a high density ratio, high viscosity, and weak surface tension forces compared to water-air systems, careful calibration of solver parameters, mesh division, and time step are essential to minimize spurious currents while preserving interface curvature accuracy.

1 Introduction

Soil is a multiphase porous media with solid grains, liquids, vapors, gases, and solidified fluids in the pore space. The fluid composition in the pores varies with temperature and pressure, affecting soil's mechanical properties [1]. The effective stress principle based on the continuum approach has limitations for partially saturated soils, necessitating examination of forces at the particle scale [2].

This study employs a micromechanical CFD approach to examine the forces exerted on the soil particles by a dis crete capillary bridge, simulating the pendular regime in partially saturated soils. The research focuses on the oil air phase, the second most commonly found fluid combination, while addressing the challenges of minimizing parasitic viscous forces in multiphase simulations using various ST models to develop accurate numerical models.

2 Micromechanical model development

A two-sphere system is studied. The fluid domain illustrated in Figure 1a is initialized with zero pressure and velocity. A structured HEX mesh is adopted with a refinement region (Figure 1b) between the spheres, where the capillary bridge is expected to form. The mesh division adopted in this study is shown in the Table 1. The fluid properties are detailed in Table 2. Oil is initialized at time t=0 s, as shown in Figure 2a, which evolves to form a stable capillary bridge at the end of 0.1 seconds in real-time, as shown in Figure 2b. The specified contact angle (30°) in the simulation develops, as illustrated in Figure 3a. The effect of gravity is neglected.

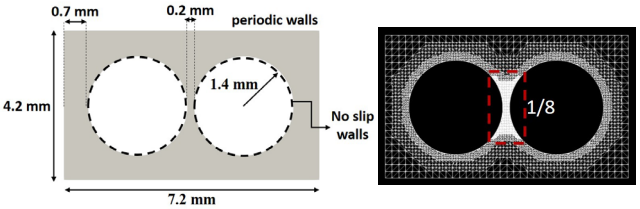

Figure 1: (a). Cross-section (x-x) of the fluid domain and boundary conditions for a two-sphere system, (b). Meshing (showing regions of refinement)

OpenFOAM Finite Volume Method (FVM) software is used for multiphase simulations. The bridge curvature and the forces acting (Figure 3b) on the two-sphere system are validated with the toroidal approximation in combination with the Young-Laplace analytical solution (Table 3). The pressure jump is given by the Young-Laplace equation (Eq. 1). The pressure jump is negative because the capillary bridge interface curves inward toward the liquid phase, creating a lower pressure inside the liquid relative to the surrounding gas phase.

$$\Delta P = -\gamma\left(\frac{1}{M.T.R} - \frac{1}{R.A}\right) \tag{1}$$

The toroidal approximation for the capillary bridge curvature between two spherical particles is (Figure 4) as follows: Radius of Arc

$$R.A = \frac{h^* + 1 - \cos\phi}{\cos(\phi + \theta)} \tag{2}$$

Mid-Toroid radius

$$M.T.R = \sin\phi - \frac{[1 - \sin(\phi + \theta)][h^* + 1 - \cos\phi]}{\cos(\phi + \theta)} \tag{3}$$

Where h^* represents the normalization of the half-separation distance with respect to the radius of the sphere, θ is the contact angle, ϕ is the half-fill angle, and R is the radius of the spherical particle.
The normal component of pressure force is given by Eq. 4

$$F^x_{\Delta p} = \pi R^2 \Delta P \sin^2 \phi \tag{4}$$

The normal component of surface tension force is given by Eq. 5.

$$F^x_{\gamma} = 2\pi\gamma R \sin\phi \sin(\phi + \theta) \tag{5}$$

For multiphase simulations, the VoF method is preferred over the Euler-Euler approach as the VoF front-capturing technique employs a single set of mass and momentum conservation equations with volume fraction (α) to indicate the presence of each fluid in the computational cells:

$$\begin{cases} \alpha = 1 & \text{oil} \\ 0 < \alpha < 1 & \text{interface} \\ \alpha = 0 & \text{air} \end{cases}$$

A ST model is also required to estimate the surface tension force in the Navier Stokes equation. OpenFOAM uses the basic Continuum Surface Force (CSF) ST model, which implements surface tension as a volumetric force acting on the fluid elements in the interface region. Algebraic VoF- Multidimensional Universal Limiter with Explicit Solution (MULES) and Geometric VoF involving interface reconstruction- Piecewise Linear Interface Calculation (PLIC) and isoAdvector (all three adopting CSF ST model) [4] is implemented for a two-sphere system. MULES ensures boundedness of the α field ($0 \leq \alpha \leq 1$) through a predictor-corrector approach where an initial unbounded solution is corrected using a flux limiter function. PLIC reconstructs the interface within each cell as a plane whose normal position is determined from the volume fraction and isoAdvector reconstructs the interface using iso-surface for $\alpha = 0.5$. The total force predictive capability is investigated as the multiphase simulations face the issue of parasitic currents, which cause parasitic viscous forces on the particles. These non-physical currents are generated due to inaccuracies in calculating the surface tension and pressure force due to the non-sharp nature of the interface (in α field) in practical VoF implementations.

Table 1: Mesh Discretization

mesh refinement	w.r.t distance between the particles
5E-5 m	1/4 (coarse)
2.5E-5 m	1/8 (medium)
1.25E-5 m	1/16 (fine)

Table 2: Properties of Oil and Air

Property	Oil	Air
Kinematic viscosity (m^2/s)	4×10^{-5}	1.48×10^{-5}
Density (kg/m^3)	850	1
Surface tension (γ) (N/m)	0.03	

3 Results and discussions

For the CSF VoF Model, medium mesh refinement was optimal. It was also observed that the coarse mesh diffused the capillary bridge, and the finer mesh increased the magnitude of the parasitic current velocity. The maximum Courant number was less than 1 for all the simulations, and the time step criterion [3] for stable multiphase simulations is given by Eq. 6

$$\Delta t \leq \max(10\tau_\mu, 0.1\tau_\rho) \tag{6}$$

where, $\tau_\mu = \frac{\mu \Delta x}{\gamma}$ and $\tau_\rho = \sqrt{\frac{\rho \Delta x^3}{\gamma}}$ represent viscous and inertial time scales, respectively (μ is dynamic viscosity, Δx is the mesh division). This criterion accounts for surface tension effects and viscous damping.

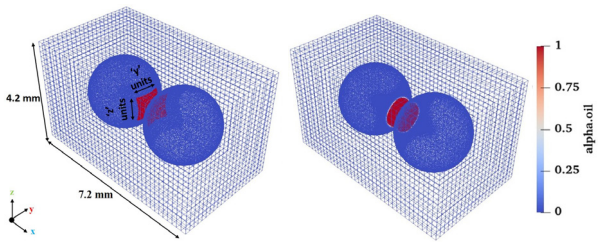

(a) **(b)**

Figure 2: (a) Bridge domain, (b) Liquid (Oil) initialized at $t = 0$ s. The coordinate system and legend are shown without labels.

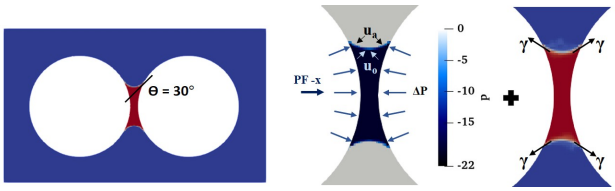

(a) **(b)**

Figure 3: (a). Cross-section (x-x) - contact angle formed at the interface, (b). Forces acting on the spherical particles due to capillary bridge formation- Pressure force +Surface Tension force

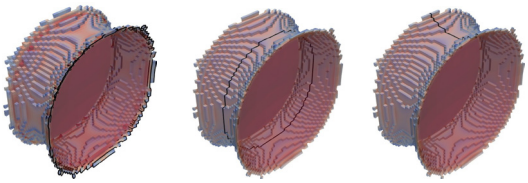

(a) W.R **(b)** M.T.R **(c)** R.A

Figure 4: Capillary bridge curvature extraction from ParaView post processing

The volume of the capillary bridge is calculated by integrating the region with α from 0.5 to 1. The interface curvature is calculated with the threshold of $\alpha \geq 0.5$, and the curvature of the best fit circle is (Figure 4) compared

Table 3: Capillary bridge curvature and analytical force according to Toroidal approximation and Young Laplace solution

Vol. (m^3)	**W.R (m)**	**M.T.R (m)**	**H.F.A**	**R.A (m)**	**S.T.F (N)**	**PF-x (N)**	**PF-y (N)**	**VF-x (N)**	**VF-y. (N)**
3.22E-10	5.81E-04	5.08E-04	24.5°	3.89E-04	8.80E-05	1.90E-05	0	0	0

Vol. = Volume, W.R = Wetting Radius, M.T.R = Mid Toroidal Radius, H.F.A = Half Filling Angle, R.A = Radius of Arc, S.T.F = Surface Tension Force, PF = Pressure Force, VF = Viscous Force.

Table 4: Interface Curvature and Total Force predictive capability of various VoF Solvers (corresponding percentage error w.r.t toroidal approximation and Young-Laplace solution at the end of 0.1s real time is also mentioned)

Parameters	CSF	SCSF_5 smoothing iterations	PLIC	isoAdvector
Volume (m^3)	3.19E-10 (-1.1%)	2.95E-10 (-8.5%)	3.20E-10 (-0.9%)	3.20E-10 (-0.9%)
Mid-Toroid Radius (m)	5.31E-04 (4.5%)	4.94E-04 (-2.8%)	5.37E-04 (5.7%)	5.37E-04 (5.7%)
Half filling angle	24.6° (0.4%)	22.3° (-8.9%)	24.3° (-0.8%)	25° (2.0%)
Radius of Arc (m)	4.25E-04 (9.1%)	3.88E-04 (-0.3%)	4.06E-04 (4.3%)	4.00E-04 (2.9%)
Surface Tension force (N)	8.83E-05 (0.4%)	8.06E-05 (-8.4%)	8.73E-05 (-0.8%)	8.96E-05 (1.8%)
Normal Pressure Force (N)	2.28E-05 (20.0%)	2.02E-05 (6.5%)	2.94E-05 (54.7%)	2.30E-05 (21.1%)
Tangential Pressure Force (N)	8.23E-08 (100%)	6.21E-06 (100%)	2.28E-07 (100%)	1.39E-07 (100%)
Normal Viscous Force (N)	9.66E-05 (100%)	2.62E-05 (100%)	1.14E-04 (100%)	9.91E-05 (100%)
Tangential Viscous Force (N)	2.13E-05 (100%)	1.15E-05 (100%)	1.20E-05 (100%)	1.65E-05 (100%)
Total Normal Force (N) (PF-x + VF-x)	1.19E-04 (528.2%)	4.64E-05 (144.5%)	1.43E-04 (653%)	1.22E-04 (542.8%)

Table 5: Sensitivity of SSF ST model predictions to different Sharpening Coefficients (corresponding percentage error w.r.t toroidal approximation and Young-Laplace solution at end of 0.1s real time is also mentioned)

Parameters	SSF_0.001 (fine mesh)	SSF_0.01 (fine mesh)	SSF_0.1 (fine mesh)
Volume	3.04E-10 (-5.6%)	3.04E-10 (-5.7%)	3.04E-10 (-5.6%)
Mid-Toroid Radius (m)	5.21E-04 (2.5%)	5.22E-04 (2.7%)	5.24E-04 (3.1%)
Half filling angle	24.3° (-0.8%)	24.4° (-0.3%)	24.3° (-0.7%)
Radius of Arc (m)	4.10E-04 (5.3%)	4.18E-04 (7.4%)	5.10E-04 (31.0%)
Surface Tension force (N)	8.73E-05 (-0.8%)	8.77E-05 (-0.3%)	8.73E-05 (-0.8%)
Normal Pressure Force (N)	2.19E-05 (15.0%)	1.96E-05 (2.9%)	1.49E-05 (-21.7%)
Tangential Pressure Force (N)	2.07E-08 (100%)	5.44E-08 (100%)	6.58E-08 (100%)
Normal Viscous Force (N)	8.28E-07 (100%)	2.26E-06 (100%)	4.27E-05 (100%)
Tangential Viscous Force (N)	1.32E-08 (100%)	1.03E-06 (100%)	7.91E-06 (100%)
Total Normal Force (N) (PF-x + VF-x)	2.27E-05 (19.4%)	2.18E-05 (14.8%)	5.76E-05 (203.0%)

with the toroidal approximation. The error in the calculation of the Surface Tension force is similar to the error of the Wetting Radius. While the Geometric VoF method demonstrated better volume conservation, it still failed to produce reliable total force and capillary bridge curvature prediction. Also, the Algebraic VoF approach showed inadequate capabilities Table 4).

Advanced Surface Tension (ST) models were imple mented to reduce errors in interface curvature estimation and improve total force prediction capabilities in the MULES VoF solver. The Smoothed Continuum Surface Force (SCSF) approach, which applies Laplacian smooth ing to the α field only for calculating unit normal vectors and curvature, significantly reduced noise in the normal vector field. This enhancement improved MULES' total normal force (normal pressure force + normal viscous force) prediction capability from a 528% error to 144.5%. Five smoothing iterations proved optimal for maintaining interface sharpness while improving accuracy for the two-sphere model oil-air fluid combination. It's also important to note that these smoothing iterations require further tuning based on the curvature complexity.

For the SCSF ST model, the surface tension force prediction accuracy was reduced to −8.4%, indicating the need for better curvature prediction while smoothing the α field. Hence, sharpening the volume fraction field with smoothing was achieved through the Sharp Surface Force (SSF) ST model to give reliable results. For the oil-air fluid combination, the SSF advanced ST model performed better with a finer mesh (mesh refinement of $1/16^{th}$ of the distance between the spheres), an adaptive maximum time step of 1E-5 seconds, and a maximum Courant number of 0.8. In the VoF approach using the CSF model, the discrete nature of the computational grid causes the interface to be represented as a staircase rather than a smooth curve, introducing further errors in curvature calculation using the CSF model. This increases the velocity of the spurious currents on mesh refinement. However, for the SSF ST model on refining the mesh, a reduction in spurious current velocity is observed due to smoothing and sharpening of α field.

The SSF ST model also requires careful tuning of the sharpening coefficient (Cpc) as it controls the sharpness of capillary pressure transitions at the interface and depends on the fluid combination. For the oil-air system, the optimal Cpc was 0.01. The error in total normal force prediction decreased from 528% for the CSF ST model to 14.8% for the SSF ST model. The capillary bridge curvature and surface tension force prediction accuracy also improved. The parasitic viscous forces were further reduced by reducing the Cpc to 0.001, but the normal pressure force prediction was compromised. However, on increasing the Cpc, the accuracy was drastically reduced (Table 5).

Although the parasitic current velocity is lower in the oil-air phase than in the water-air phase, the parasitic viscous forces are comparatively greater in oil-air systems. This can be explained through the capillary number (Ca), a dimensionless parameter that represents the ratio of viscous forces to surface tension forces (Eq. 7). Analyzing the parasitic current velocity of the oil phases (the oil phase contributes significantly to the viscous parasitic forces), it is observed that the combination of oil and air fluid exhibits higher Ca in all the solvers tested (Table 6).

$$\mathrm{Ca} = \frac{\rho \nu U}{\gamma} \tag{7}$$

where, ρ is the fluid density [kg/m^3], ν is the kinematic viscosity of the fluid [m^2/s], U is the characteristic velocity [m/s], γ is the surface or interfacial tension [N/m].

Table 6: Capillary Number for different VoF solvers - solver parameters producing the least parasitic viscous force for the respective fluid combinations is used in this comparison ($U_{\max}$ in m/s)

	$\mathrm{Ca}_{\text{Oil-air}}$	$\mathrm{Ca}_{\text{Water-air}}$	$(U_{\max})_{\text{oil}}$	$(U_{\max})_{\text{water}}$
CSF	6.5E-03	2.3E-03	5.7E-03	1.6E-01
PLIC	1.5E-02	1.4E-02	1.3E-02	1.0E+00
isoAdv	1.7E-02	5.5E-03	1.5E-02	3.9E-01
SCSF	1.5E-02	3.3E-03	1.3E-02	2.3E-01
SSF	7.4E-03	5.4E-04	6.5E-03	3.8E-02

4 Conclusions

This study demonstrates the significant improvements in interface curvature estimation by implementing the SSF ST model for oil-air fluid combination. The SSF ST model improved total normal force prediction accuracy with error rates decreasing from 528% for the CSF ST model to 14.8% and the Surface Tension force to -0.3%. The effectiveness of these improvements is contingent upon the proper tuning of solver parameters. The optimal Cpc value for the oil-air phase is 0.01, possibly due to the relatively weaker surface tension force than the water-air fluid combination [5] (with an optimal Cpc of 0.3).

References

[1] 47th Rankine Lecture 21 March 2007, Géotechnique, 60(1), 1-1 (2010). https://doi.org/10.1680/geot.9.B.011

[2] Fredlund, D.G. State Variables in Saturated Unsaturated Soil Mechanics. Soils and Rocks 39(1), Special Issue: Unsaturated Soils, January-April 2016. https://soilsandrocks.com/sr-391003

[3] Gamet, L., Scala, M. Validation of volume-of-fluid OpenFOAM® isoAdvector solvers using single bubble benchmarks,Computers and Fluids, 104722 (2020). https://doi.org/10.1016/j.compfluid.2020.104722

[4] Vachaparambil, K. J, On sharp surface force model: Effect of sharpening coefficient, Experimental and Computational Multiphase Flow, 226–232 (2021). https://doi.org/10.1007/s42757-020-0063-5

[5] Manjunath, K., Reducing Parasitic Viscous Forces in the Pendular Liquid Bridge Simulation (Imperial College London Dissertation, 2024).